FREEFORM FABRICATION OF ZIRCONIUM DIBORIDE PARTS USING SELECTIVE LASER SINTERING

Ming C. Leu[1], Erik B. Adamek[1], Tieshu Huang[2], Greg E. Hilmas[2] and Fatih Dogan[2]

[1]Department of Mechanical and Aerospace Engineering

[2]Department of Material Science and Engineering

Missouri University of Science and Technology

Rolla, MO 65409

{mleu@mst.edu, ebawc3@mst.edu, hts@mst.edu, ghilmas@mst.edu, doganf@mst.edu}

Reviewed, accepted September 10, 2008

ABSTRACT

Using the Selective Laser Sintering (SLS) process, both flexural test bars and 3D fuel injector components have been fabricated with zirconium diboride (ZrB_2) powder. Stearic acid was selected as the binder. Values of SLS process parameters were chosen such that the green parts could be built with sharp geometrical features and that the sintered parts could have good mechanical properties. After binder burnout and sintering, the SLS fabricated ZrB_2 test bars achieved 80% theoretical density, and the average flexural strength of the sintered samples was 195 MPa. These values demonstrate the feasibility of the SLS process for freeform fabrication of 3D parts with the ultra high temperature ceramic.

1. INTRODUCTION

Complex three-dimensional shapes are not always a viable option from ceramic materials using conventional manufacturing techniques. In addition to high failure rates in machining operations such as drilling and milling due to brittleness of ceramic materials, some geometric features like internal voids and curved holes are impossible to create by these and other conventional methods. Moreover, the costs associated with conventional construction of 3D parts rises sharply for ceramic materials with increasing geometric complexity of the part.

Several solid freeform fabrication (SFF) techniques have been researched for fabricating parts with ceramic materials. These techniques include Fused Deposition of Ceramics [Rangarajan et al., 2000; Lous et al., 2000; Bandyopadhyay et al., 2000; Danforth et al., 2002], Fused Deposition Modeling [Crump, 1992], Extrusion Freeform Fabrication [Hilmas,1996; Wang, 2004; Huang et al., 2006; Zhao et al., 2007], slurry and binder-based 3-D Printing [Cima et al., 2001], Chemical Liquid Deposition [He and Zhou, 2000], Selective Laser Sintering [Deckard, 1989; Beaman et al., 1997], Selective Laser Melting [Kruth et al., 2004; Klocke and Ader, 2003], Shape Deposition Manufacturing [Cooper et al., 2002; Stampfl et al., 2001], and Robocasting [Cesarano, 1999]. Although these techniques have been demonstrated for layer-by-layer freeform

fabrication of ceramic components, many technical challenges remain, especially for SFF of ultra high temperature ceramics (UHTCs).

Selective Laser Sintering (SLS) holds two unique advantages compared with other SFF processes: one is the wide variety of materials that can be used in SLS processing, and the other is no need for building, and subsequently removing, support structures in fabricating complex 3D parts. In the SLS process, the STL file of a solid model is sliced into layers of specified thickness. The contours of each layer are transferred to the process controller of an SLS machine, which actuates servo mirrors to direct a laser beam to outline and fill in the two dimensional profile of a layer. After each layer is completed, the build area lowers by one layer thickness and fresh powder is spread over the build area. The layer fabrication step repeats until the entire part has been built. After finishing the build, the part cake is removed and broken to obtain the built part. In SLS of ceramics, the fabricated green part is further processed for binder burnout and subsequent sintering to achieve high relative density and mechanical strength. A comprehensive discussion of consolidation phenomena in SLS (and its variants) of various types of materials is given by Kruth et al. [2007].

Zirconium Diboride (ZrB_2) is an ultra high temperature ceramic with a melting temperature of 3245 °C, a flexural strength of 200-590 MPa, and a hardness of 21-23 GPa [Fahrenholtz et al., 2007]. It has high electrical and thermal conductivity as well as excellent chemical resistance and thermal shock resistance [Bellosi and Monteverde, 2002; Fahrenholtz et al., 2007]. ZrB_2 is an excellent candidate for a number of ultra high temperature applications, such as rocket propulsion nozzle throat inserts and leading edges of future-generation hypersonic space vehicles. However, since ZrB_2 cannot be cast using traditional forming processes, due to its extremely high melting temperature, current processing techniques are limited to pressure-assisted and pressureless sintering followed by post-process machining. Not only the brittleness of material limits the scope and success rate of the post-process operations, but the rate of manufacture is necessarily low in order to reduce the chances of failure.

Previous research on SLS of ZrB_2 powder included a study by Stucker et al. [1995, 1997] to develop a new way of manufacturing electrical discharge machining (EDM) electrodes. ZrB_2 green parts were fabricated by SLS, followed by debinding, sintering, and infiltration with copper to make EDM electrodes. The sintered ZrB_2 parts were 31% dense on average before Cu infiltration. There have been no mechanical properties reported for these sintered parts. Another study of laser sintering of $ZrB_2$was performed by Sun and Gupta [2008], who reported that ZrB_2 powder having small particle size improved surface wetability and sinterability.

The present paper describes an experimental study of using the SLS process to fabricate ZrB_2 components. The experiments involved consideration of materials, SLS process parameters, binder burnout, and sintering. The process was developed to fabricate ZrB_2 samples including flexural test bars and 3D fuel injector components. The dimensions of both green and sintered test bars were measured and compared with nominal dimensions. The measured dimensions, density and flexural strength of the test samples are presented and discussed.

2. EXPERIMENTS

2.1 Materials and Powder Preparation

The material used was zirconium diboride powder (grade B, H.C. Starck, Karlsruhe, Germany) with an average particle size of 2-3 μm and a relative surface area of 1.38 m^2/g (8.42 m^2/cm^3). The as-received ZrB_2 powder had an oxygen content of 0.9 wt.%. Boron carbide (B_4C; grade HS, H.C. Starck) having an average particle size of 0.8 μm and a surface area of 15.8 m^2/g (39.82 m^2/cm^3) was used as a sintering additive. The oxygen content of the B_4C additive was about 1.3 wt.%. Carbon black (Black pearls 120, Cabot Corporation, Alpharetta, GA) was used as a source of carbon (C). Stearic acid (Acros Organics, Stearic Acid, 97% New Jersey) was used as the binder.

To prepare ZrB_2 powder for use in the SLS process, first the powder was mixed with sintering additives (1 wt.% B_4C and 0.2 wt.% C) by ball milling for a period of 24 hours. These additives promote full sintering during the post-SLS sintering process. After the ceramic and additives were mixed thoroughly, stearic acid was added at 50:50 vol.% and ball milled for an additional period of at least 24 hours. Stearic acid was chosen as the binder for the ZrB_2 powder based on the result of a previous study performed for SLS of Al_2O_3 powder [Liu et al., 2007]. Stearic Acid has a number of beneficial properties for use as the binder. It is a thermoplastic and the change in its state from a solid to a liquid yields only a small change in density. This reduces curling in the part bed and contributes to more successful lamination. Stearic acid does not react with ZrB_2 and the powder can be reused several times. The low melting temperature of the binder adds to its SLS friendliness. The 50:50 ZrB_2/stearic acid mixture was used for the SLS process after the initial 55:45 ZrB_2/stearic acid mixture yielded no successful fabrication.

The mixed powder was then checked for clumping, which may occur if the humidity and temperature are high due to the waxy nature of stearic acid. Problems faced during powder processing included some batches of powder agglomerating into a ball or a ring of powder as shown in Figure 1. These clumps were crushed and re-milled to return to powder form. The differences between batches were the ambient humidity and temperature. The moisture content has the largest effect, causing the powder to clump together perchance during SLS processing.

(a) (b)

Figure 1: Clumps of powder (a) ball and (b) ring

2.2 SLS Processing and Process Parameters

The SLS system used was a DTM 2000 Sinterstation shown in Figure 2. Core features of this machine include heated powder feed bins as well as heating of the part piston. A 50W CO_2 laser was used to introduce beam energy into the part bed by selectively directing laser beam onto the surface of the part bed. Preparation of the setup for SLS processing involved placing .STL files for the parts into the Sinterstation software package, setting all process parameters, filling the feed bins with powder, and sealing and evacuating the O_2.

The values of SLS process parameters were selected by a combination of theoretical calculations, analytical reasoning, and empirical testing. The temperature of the powder feed bins must be low enough so that the binder is not sticky while high enough so that it can heat the powder quickly in the build area. The part piston and part bed temperatures need to be close to the melting temperature of stearic acid (69°C) so that the laser does not need to excite the powder temperature to such a degree that curling due to the change in density as a result of temperature gradient becomes inevitable. A temperature that is too high, however, may result in one fused piece. The layer thickness at 0.0762 mm is the smallest layer thickness available from the Sinterstation. This thickness was chosen because the layers did not laminate together when the thickness was set any higher, due to the limited penetration ability of laser in ZrB_2 powder.

The laser power (W) is related to the process parameters as follows:

$$W = k \times \Delta T \times \left[\left(p_1 H_{c1} \times p_2 H_{c2} \right) + H_{f2} \right] \times ScanSpeed \times ScanSpacing \times LayerThickness$$

where ΔT is the change in temperature, p_x is the volumetric percentage of material x, H_c is the heat capacity of material x, H_f is the heat of fusion of the binder, and *k* is a coefficient depending on powder density, reflectivity, etc. A series of experiments were conducted to determine the scan speed and laser power. The experiments indicated that the laser has limited penetration ability in ZrB_2 powder, thus the laser scan speed has to be decreased substantially from that previously used in SLS of Al_2O_3 [Liu et al., 2007] in order to generate sufficient binder fusion and avoid delamination between layers. The amount of energy required was determined assuming perfect absorption by the powder and no significant heat dissipation, thus the calculation serves as a low estimate of the necessary power setting and is a first approximation.

Based on the above considerations, the following SLS process parameters were chosen for fabricating ZrB_2 parts: part bed temperature 59°C, part piston temperature 48°C, feed bin temperature 25°C, laser scan speed 50.8 mm/s, scan spacing 0.152 mm, layer thickness 0.0762 mm, and laser power from 0.8 to 1.0 watt. With this set of parameters the SLS process yielded 15 flexure test bars and 7 injector parts, representing an overall yield of 17%.

Figure 2: DTM 2000 Sinterstation

ZrB_2 parts fabricated by the Sinterstation were broken out using a combination of mechanical brushing for rough breakout and compressed air around 10 psi for fine surface cleaning. The green parts were inspected visually for possible delamination and fracture during the fabrication process. Figure 3 shows the ZrB_2 powder bed with 12 fused parts during the SLS processing. The absence of curling and the change in color due to the vaporization of stearic acid indicates that the SLS process was going smoothly. However, the quality of lamination between layers cannot be judged by visual observation during the fabrication process. The acceptability of layer-to-layer lamination can only be determined after part breakout. Figure 4 shows the sharp features of green ZrB_2 test bars after SLS processing.

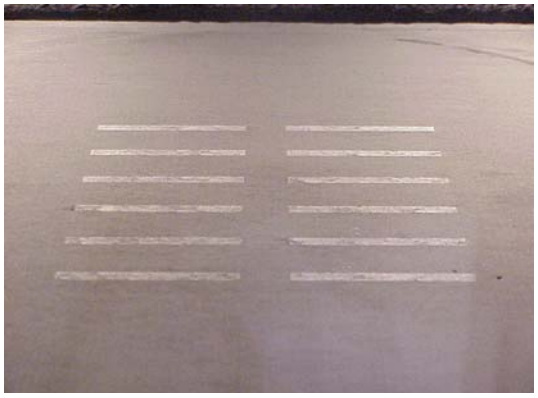

Figure 3: ZrB_2 test samples in the powder bed during SLS processing

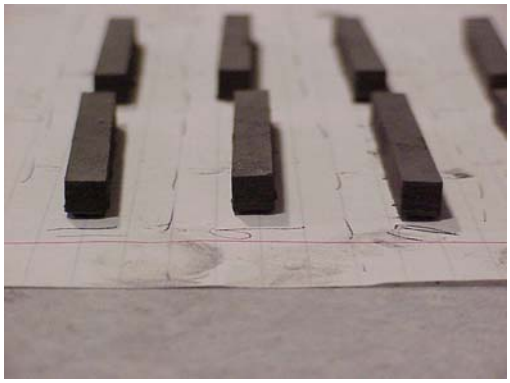

Figure 4: Green ZrB2 test bars after SLS processing

2.5 Binder Burnout and Sintering

Binder burnout for the green ZrB_2 parts was performed in a furnace using the temperature profile shown in Figure 5. The parts were slowly brought to a temperature of 600°C. The ramp time for reaching this temperature was chosen specifically to be very long in order to allow vacating the binder completely from the part without bloating or cracking. The process took about 52 hours. It removed all of the organic species and allowed for some rearrangement of the ceramic particles (resulting in a minimal amount of shrinkage). The binder burnout for ZrB_2 samples was accomplished in an environment of 10% H_2 and 90% Ar. This environment was used to remove the binder without unwanted oxidation of the ZrB_2 powder. The binder burnout process had a 100% yield.

The green test bars underwent isostatic pressing before the binder burnout. The isostatic pressing was done by vacating the air in a nitrile glove with parts located at the fingers and dipping the glove into the isostatic pressing bath at 276 GPa for 1 min. It was used to increase the green densities of the parts in order that higher sintering densities can be achieved. This process had a 100% yield.

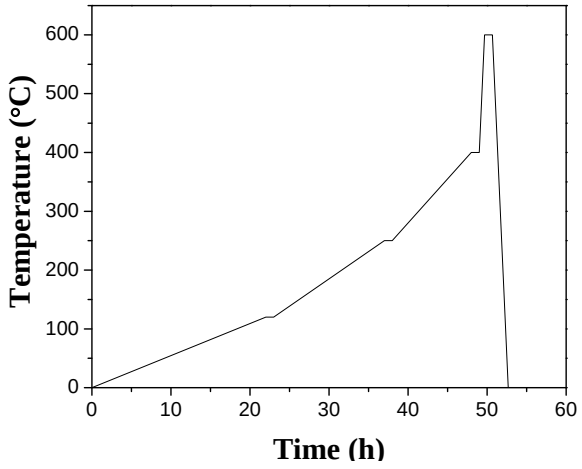

Figure 5: Binder burnout schedule for ZrB_2 samples

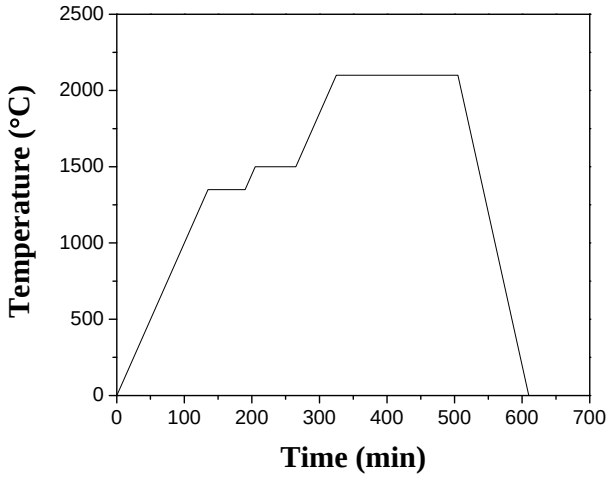

Figure 6: Sintering schedule for ZrB_2 samples

Final sintering of ZrB_2 parts was performed at 2,200°C, which was maintained for 2 hours in a Lindberg graphite furnace (model 51644). The parts were then cooled at a rate of 10 ˚C/min. The sintering schedule is shown in Figure 6. The sintering process took about 10 hours, and it had a 100% yield.

3. RESULTS

To study the physical properties and microstructures of SLS processed ZrB_2 parts, flexural test bars and 3D fuel injector components were fabricated using the Sinterstation. The green parts then underwent binder burnout and sintering. Figure 7 shows a green ZrB_2 test bar and the same bar after sintering. Figure 8 shows a fuel injector part viewed in two different directions and the same part after sintering.

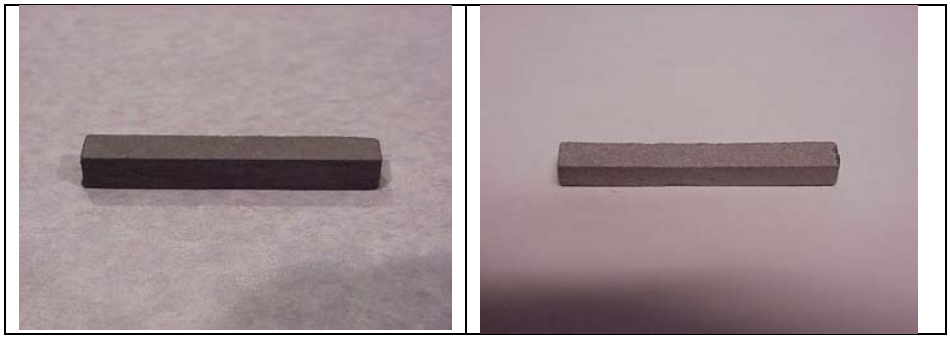

(a) (b)

Figure 7: A ZrB_2 flexural test bar made by SLS: (a) green part and (b) after sintering. The dimensions are: for the green part, X=51.8 mm, Y=6.8 mm, Z=6.2 mm; for the sintered part, X=42.0 mm, Y=5.2 mm, Z=3.7 mm.

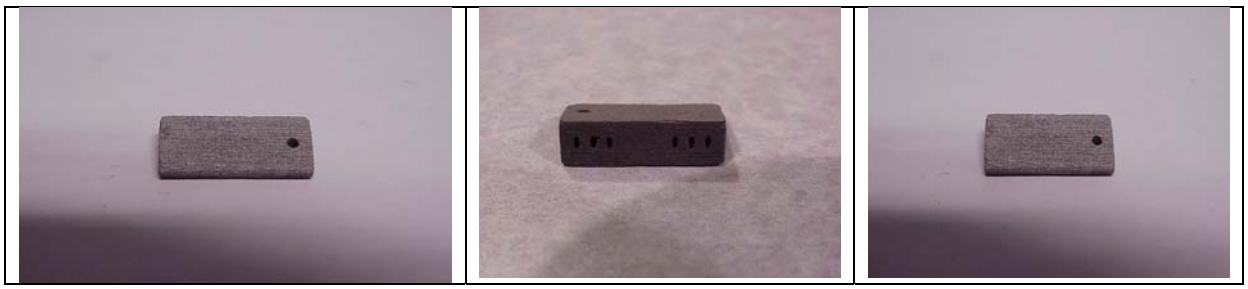

Figure 8: A ZrB_2 3D test part made by SLS: (a) green part, (b) another view of the test part, and (c) after sintering. The dimensions are: for the green part, X=25.4 mm, Y=12.9 mm, Z=7.4 mm; for the sintered part, X=21.4 mm, Y=10.5 mm, Z=4.8 mm.

Table 1: Nominal dimensions and physical dimensions of the test bar

Part No.	X Nominal (mm)	Y Nominal (mm)	Z Nominal (mm)	Green			Sintered		
				X Dim. (mm)	Y Dim. (mm)	Z Dim. (mm)	X Dim. (mm)	Y Dim. (mm)	Z Dim. (mm)
1	51.97	6.6	6.75	51.9	6.9	6.7	42.2	5.4	4.4
2	51.97	6.6	6.75	52.0	6.8	6.8	42.3	5.3	4.3
3	51.97	6.6	6.75	52.0	7.0	7.0	42.7	5.3	4.6
4	51.97	6.6	6.75	52.0	6.8	6.5	42.1	5.3	4.0
5	51.97	6.6	6.75	52.0	6.9	6.2	42.4	5.3	3.9
6	51.97	6.6	6.75	52.0	6.8	6.7	42.2	5.3	4.2
7	51.97	6.6	6.75	51.9	6.8	6.6	41.9	5.1	3.8
8	51.97	6.6	6.75	51.9	6.8	6.7	42.1	5.1	3.8
9	51.97	6.6	6.75	51.9	6.8	6.4	42.0	5.2	3.7
10	51.97	6.6	6.75	51.8	6.8	6.2	42.0	5.2	3.7
11	51.97	6.6	6.75	51.9	6.8	6.2	42.0	5.2	3.7
12	51.97	6.6	6.75	51.9	6.8	6.6	42.3	5.2	3.9
13	51.97	6.6	6.75	51.9	6.8	6.3	42.3	5.2	3.6
14	51.97	6.6	6.75	51.8	6.8	6.7	42.1	5.2	3.9
Mean	51.97	6.6	6.75	51.92	6.83	6.54	42.19	5.24	3.96
Standard Deviation	-	-	-	0.08	0.06	0.24	0.22	0.08	0.29

Table 2: Dimensions of the green and sintered test bars as percent of nominal dimensions

		X	Y	Z
Green Part	% of nominal	100	103	97
	std. deviation (% of nominal)	0.16	0.90	3.59
Sintered Part	% of nominal	81	79	59
	std. deviation (% of nominal)	0.41	1.25	4.30

The manufactured parts were measured for both the green and sintered parts. Table 1 shows the dimensions measured from the 14 successfully sintered test bars against nominal dimensions. Table 2 shows the dimensions of the green and sintered test bars in percentage of the nominal dimensions. Note that X was along the scanning direction, Y was perpendicular to the scanning direction, and Z was in the depth (vertical) direction. All test bars were fabricated so that the longest dimension was the direction of laser travel (i.e. X direction). The data in these two tables indicates that the X dimension measured from the green test bars was only 0.1% difference on average from the nominal

dimension, and that the Y and Z dimensions measured from these test bars were less than 4% different from the nominal dimensions on average. After sintering, the part shrank to about 80% of the nominal dimensions in the scanning plane (both along and perpendicular to the scanning direction) and about 60% of the nominal dimension in the depth direction. These results indicate that there is significantly more fusion in the laser scanning plane and less fusion in the depth direction. Consequently, more shrinkage occurred in the depth direction during sintering.

After sintering, the densities of ZrB_2 test bars were measured using Archimedes method. The average density measured of the sintered test bars was 4.87 g/cc, which is 80% theoretical density. This is much higher than the 31% theoretical density previously reported [Stucker, 1997]. The density of sintered part is affected by the ceramic/binder ratio in the powder mixture and the ZrB_2 particle size. In our study, we had the 50:50 ratio of ZrB_2/stearic acid in the powder mixture. The ZrB_2 powder as received had ~3 μm in particle size, and the particles were not attrition milled. Attrition milling can significantly reduce the particle size and increase the sintering drive force for densification because smaller particles provide more surface areas overall. A larger surface area is associated with a higher surface energy, which is the major driving force for pressureless sintering.

Figure 9 shows the microstructures from a fracture surface of a test bar in two different magnifications. It can be seen that the microstructure is fairly uniform and that the pores are on the order of several microns to about ten microns in size. The fracture path is predominantly transgranular, indicating that the fracture is a typical type of brittle fracture as expected.

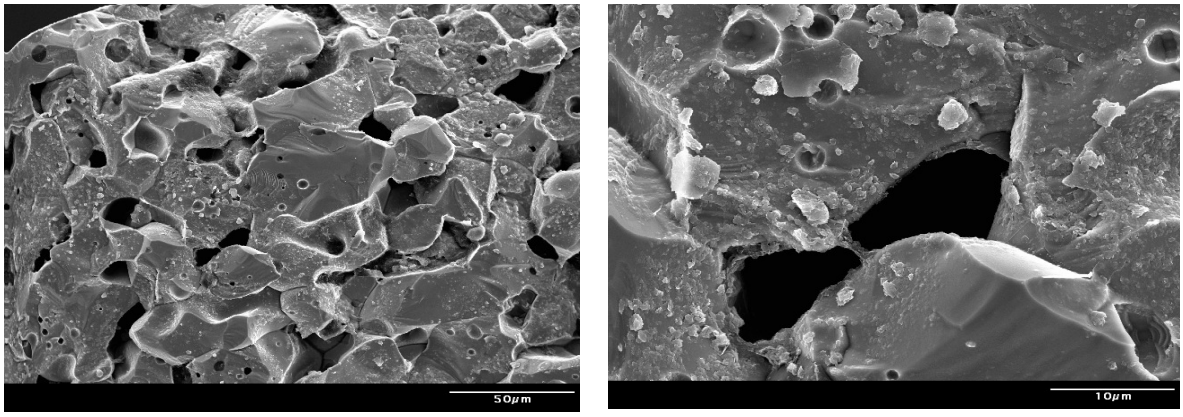

Figure 9: Microstructures of a test bar in two different magnifications

The flexural strength was measured from the 14 sintered test bars using the four point bending method. All test bars were ground to “A” bar size per ASTM standard C1161 “Standard Test Method for Flexural Strength of Advanced Ceramics at Ambient Temperature.” This standard has the test bar’s cross-sectional area of 2.0 mm by 1.5 mm (±0.05mm). By using an Instron machine, the flexural strength data was measured and collected as given in Table 3. The mean flexural strength measured from these test bars was 195 MPa, which is 44% of the flexural strength of 444 MPa obtained from hot

pressed ZrB_2 [Chamberlain et al., 2006]. To our knowledge this is the first published result on the flexural strength of SLS fabricated ZrB_2 test bars. The relatively low strength of these test bars compared to that of hot pressed samples was associated with its relatively high porosity. The hot pressed samples after sintering had 98% theoretical density, while the SLS processed samples after sintering had 80% theoretical density. Nevertheless, the 80% theoretical density achieved in our study is much higher than the 31% theoretical density previously reported [Stucker 1997]. In order to further increase the density, our future work will include optimizing the powder/binder compositions and SLS process parameters.

Table 3: Flexure strength of the test bars

Part No.	Flexure Strength (MPa)
1	218
2	216
3	208
4	205
5	205
6	200
7	199
8	197
9	190
10	185
11	184
12	183
13	178
14	162
Mean	195
Standard Deviation	16
Hot Pressed ZrB_2	444

4. CONCLUSION

SLS processing of ZrB_2 powder with stearic acid as the binder has been studied. Flexural test bars and 3D fuel injector parts have been successfully fabricated by the SLS process using a zirconium diboride/stearic acid mixture of 50:50 vol.% with appropriately determined values for SLS process parameters including part bed and feed bin temperatures, laser scan speed, scan spacing, layer thickness, and laser power. After binder burnout and sintering, the flexural test bars achieved 80% theoretical density, which is much higher than the density of similar test bars previously reported in the literature. The average flexural strength of the sintered test bars was 195 MPa, which is 44% of the flexural strength of hot pressed ZrB_2 test bars. The SEM images from the fracture surface of the samples indicated that the microstructure was fairly uniform and the pore size was about several to ten microns.

ACKNOWLEDGMENTS

This work was supported by the Air Force Research Laboratory under Contract FA8650-04-C-5704.

REFERENCES

1 Bandyopadhyay, A., Panda, P. K., Agarwala, M. K., Danforth, S. C., and Safari, A., (2000) “Processing of Piezocomposites by Fused Deposition Technique,” Journal of American Ceramic Society, 80(6): 1366-72.

2 Beaman, J. J., Barlow, J. W., Bourell, D. L., Crawford, R. H., Marcus, H. L., and McAlea, K. P., (1997) *Solid Freeform Fabrication: A New Direction in Manufacturing*, Kluwer Academic Publishers, Norwell, MA.

3 Bellosi, A., and Monteverde, F., (2002) "Fabrication and Properties of Zirconium Diboride-Based Ceramics for UHT Applications." Proceedings of 4th European Workshop, 521: 26-29.

4 Cesarano, J. III, (1999) “A review of robocasting technology,” Solid Freeform and Additive Fabrication: a Materials Research Society Symposium; Boston, MA, pp.133-139

5 Chamberlain, A. L., Fahrenholtz, W. G., and Hilmas, G. E., (2006) “Pressureless Sintering of Zirconium Diboride,” Journal of American Ceramic Society, 89(2): 450–456

6 Cima, M.J., Oliveira, M., Wang, H.R., Sachs, E., and Holman, R., (2001) “Slurry-Based 3DP and Fine Ceramic Components,” Proceedings of Solid Freeform Fabrication Symposium, Austin, Texas, pp. 216-223.

7 Cooper, Alexander G., Kietzmen, John W., Prinz, Friedrich B., (2002) “Mold Shape Deposition Manufacturing,” U.S. Patent, No. 6,375,880 B1.

8 Crump, S. S., (1992) “Appartus and Method for Ceramic Three-Dimensioal Objects” U.S. Patent No. 5,121,329.

9 Danforth, S. C., Agarwala, M., Bandyopadghyay, A., Langrana, N., Jamalabad, V. R., Safari, A. and Van Weeren, R., (1998) “Solid Freeform Fabrication Methods,” U.S. Patent No. 5,738,817.

10 Deckard, C., (1989) "Method and Apparatus for Producing Parts By Selective Sintering", U.S. Patent No. 4,863,538.

11 Fahrenholtz, W. G., and Hilmas, G. E., (2007) "Refractory Diborides of Zirconium and Hafnium." Journal of American Ceramic Society, 90(5): 1347-64.

12 He, Z., and Zhou, J. G., (2000) “Feasibility Study of Chemical Liquid Deposition Based Solid Freeform Fabrication,” Journal of Materials and Design, 21: 83-92

13 Hilmas, G. E., Lombardi, J. L., and Hoffman, R. A., (1996) “Advances in the Fabrication of Functional Graded Materials using Extrusion Freeform Fabrication,” Functionally Graded Materials, pp. 319-324 .

14 Huang, T., Mason, M. S., Hilmas, G. E., and Leu, M. C., (2006) “Freeze-form Extrusion Fabrication of Ceramic Parts,” International Journal of Virtual and Physical Prototyping, 1(2): 93-100.

15 Klocke, F, and Ader, C., (2003) “Direct Laser Sintering of Ceramics,” Proceedings of Solid Freeform Fabrication Symposium, Austin, Texas, pp. 447-455.

16 Kruth, J. P., Mercelis, P., Froyen, L., and Rombouts, M., (2004) “Binding Mechanisms in Selective Laser Sintering and Selective Laser Melting,” Proceedings of Solid Freeform Fabrication Symposium, Austin, Texas, pp. 44-59.

17 Kruth, J. P., Levy, G., Klocke, F., and Childs, T. H. C., (2007) “Consolidation Phenomena in Laser and Powder-Bed Based Layered Manufacturing,” Annals of the CIRP, 56(2), pp. 730-759.

18 Liu, Z. H., Nolte, J. J., Packard, J. I., Hilmas, G., Dogan, F. and Leu, M. C., (2007) “Selective Laser Sintering of High-Density Alumina Ceramic Parts,” Proceedings of 35th International MATADOR Conference, Taipei, Taiwan, pp. 351-354.

19 Lous, G. M., Cornejo, I. A., McNlty, T. F., and Danforth, S. C., (2000) “Fabrication of Piezoelectric Ceramic/Polymer Composite Transducers Using Fused Deposition of Ceramics,” Journal of American Ceramic Society, 83(1): 124-28.

20 Rangarajan, S., Qi, G., Venkataramen, N., Safari, A., and Danforth, S. C., (2000), “Powder Processing, Rheology, and Mechanical Properties of Feedstock for Fused Deposition of Si_3N_4 Ceramics,” Journal of American Ceramic Society, 83(7): 1663-69.

21 Sun, C-N., and Gupta, M. C., (2008) “Laser Sintering of ZrB_2,” Journal of American Ceramic Society, 91(5): 1729-31.

22 Stampfl, J., Cooper, A., Leitgeb, R., Cheng, Y., Prinz, F., (2001) “ Shape Deposition Manufacturing of Microscopic Ceramic and Metallic Parts Using Silicon Molds,” U.S. Patent, No. 6,242,163 B1.

23 Stucker, B. E., Bradley, W. L., Norasetthekul, S., and Eubank, P. T., (1995) “The Production of Electrical Discharge Machining Electrodes Using SLS: Preliminary Results,” Proceedings of Solid Freeform Fabrication Symposium, Austin, Texas, pp. 278-286.

24 Stucker, B. E., Bradley, W. L., Eubank, P. T., Norasetthekul, S., and Bedri, B., (1997) “Zirconium Diboride/Copper EDM Electrodes From Selective Laser Sintering,” Proceedings of Solid Freeform Fabrication Symposium, Austin, Texas, pp. 257-265.

25 Wang, J. W., Shaw, L. L., Xu, A., and Cameron, T. B., (2004) “Solid Freeform Fabrication of Artificial Human Teeth,” Proceedings of Freeform Fabrication Symposium, Austin, Texas, pp. 816-825.

26 Zhao, X., Mason, M. S., Huang, T., Leu, M. C., Landers, R. G., Hilmas, G. E., Easley, S. J., and Hayes, M. W., (2007) “Experimental Investigation of Effect of Environment Temperature on Freeze-form Extrusion Fabrication,” Proceedings of Solid Freeform Fabrication Symposium, Austin, TX, pp. 135-146.